UWB FILTERING USING HEXAGONAL HONEYCOMB SHAPED RESONATOR

Partha Protim Kalita[*1], Gouree Shankar Das[1], Akash Buragohain[1,2], Trishna Doloi[1], and Yatish Beria[1]

[1]*Microwave Research Laboratory, Department of Physics, Dibrugarh University, Dibrugarh-786004, Assam, India*
[2]*Department of Physics, Tingkhong College, Dibrugarh-786612, Assam, India*

[*]Corresponding Author: kalitapartha14@gmail.com

(Received 25 September 2025; revised 16 December 2025; accepted 22 December 2025; published 1 August 2026)

Abstract: Ultra-wideband (UWB) technology is a modern wireless communication system that uses a large amount of bandwidth. Due to its various advantages, such as high-speed data transfer, precise location detection, and secured communication, it has numerous applications in communication systems, medical imaging, automobile and radar systems etc. According to the Federal Communications Commission (FCC), in 2002, the unlicensed allowed frequency for UWB indoor and handheld applications is restricted within 3.1 GHz to 10.6 GHz. Hence, research is carried out to develop UWB filters, which are an important component of a UWB communication system to limit the frequency and reduce interference from other signals. This paper introduces a new UWB filter that uses a hexagonal honeycomb-shaped resonator. The hexagonal design not only saves space but also improves how the filter performs compared to traditional designs. Also, interdigital parallel coupled microstrip lines (PCML) are used to excite the resonator and to achieve the bandpass behaviour. We carefully designed the resonator's dimensions to achieve good performance, resulting in low insertion loss (IL) and a wide operational bandwidth. The passband of the designed filter spans from 3.14 GHz to 10.56 GHz with a fractional bandwidth of 108.32% and minimal signal loss. The filter is designed on a low-cost FR4 substrate with a dielectric constant of 4.4 and a thickness of 1.6 mm. The simulation of the filter is done using ANSYS High Frequency Structure Simulator (HFSS). Due to its compact and cost-effective design, this filter can be used in applications like communication systems and radar systems.

Keywords: UWB filter; PCML; Hexagonal resonator; Honeycomb shaped filter.

PACS: 88.80.ht, 84.30.Bv, 85.50.-n, 84.40.Dc

1 Introduction

In microwave communication systems, various components like antennas, filters, and low noise amplifiers (LNAs) are used to effectively and efficiently transmit the signals across the communication chain. Among these, filters are essential components that transmit only desired frequency signals through it while rejecting other signals. Filters can control the bandwidth, reduce noise, and improve signal integrity with enhanced performance [1, 2]. Filters can be used in a wide range of narrow-band applications like Bluetooth, Wi-Fi, and GPS for smooth signal transmission by blocking interference from outside sources [3]. But with the growth of the modern communication system, there is a need for a more stable, high-speed, high-capacity and secure system. To fill this void, ultra-wideband (UWB) technology emerges as a suitable technical evolution due to its high bandwidth capacity [4, 5]. Instead of using continuous radio waves, UWB technology uses a series of short-range and short-duration pulses to transmit signals wirelessly, making it a secure mode of communication [6]. These enable UWB technology with high data rates, precision in ranging, and imaging with low power uses, which makes it suitable for indoor, medical, and radar applications. Initially, UWB technology was used primarily for military purposes, particularly radar and secure communication [7]. But, in 2002, the U.S. Federal Communications Commission (FCC) formally allocated the unlicensed use of UWB for indoor and handheld devices in the frequency range from 3.1 GHz to 10.6 GHz with a strict power density limit of -41.3 dBm/MHz, thus creating a standardised spectral window for commercial development of UWB systems [8]. Since then, UWB has found significant use in short-range wireless networks, indoor localisation, biomedical imaging, vehicular radar systems, and next-generation IoT-enabled communication networks [9].

To operate UWB technology over a wide-ranging band, the UWB bandpass filter (BPF) plays a critical role by shaping the bandwidth (3.1-10.6 GHz), minimising insertion loss ($<$3dB), maintaining adequate return loss ($>$10dB), and providing strong out-of-band signal suppression [2, 10]. Although these filters can be theoretically implemented using lumped inductors, capacitors and resistors, it is not feasible for higher frequencies like microwaves and mm waves due to their fabrication limitation, parasitic effects and increased losses [11]. Hence, different distributed element technologies such as microstrip [12], co-planar waveguide (CPW) [13] and substrate integrated waveguide (SIW) [14, 15] are more suitable for UWB filter implementation. These technologies have gained attention due to their planar structure, ease of fabrication, low cost, and fabrication using printed circuit board (PCB) manufacturing. In microstrip technology, a single transmission line can exhibit inductor and resistor characteristics, which can help achieve the desired filtering response without the need for bulky lumped elements.

Over the past twenty years, numerous ultra-wideband filters have been developed utilising different design principles to increase their effectiveness and minimise size. One of the most common methods is using multi-mode resonators (MMR), which produce a series of different resonant frequencies within a single unit to cover a wide bandwidth [4]. Stepped impedance resonators (SIR) and stub-loaded resonators (SLR) have also been used to provide a more advanced filter response and increase control over the width of the passband [5]. Technologies such as using patterns within the ground plane, known as defected ground structures (DGS), or slight adjustments in the transmission lines, known as defected microstrip structures, have been widely used. These technologies suppress unwanted harmonics, increase filter selectivity, and provide strong rejection within the stopband area [18]. In [19], a quintuple-mode resonator for a UWB BPF has been designed, featuring a compact design with capacitively ended stubs and inter-digital coupled feed lines. An equivalent circuit analysis of the MMR-based UWB filter is performed and identified four resonant modes by coupling analysis in [20].

Alongside these techniques, there has been a focus on more sophisticated and innovative resonator geometries aimed at achieving reduced size and weight, while maintaining robust performance filters. Interdigital resonators, resembling a configuration of interleaved fingers, have demonstrated significant capability in providing effective electromagnetic coupling within an exceptionally compact structure, facilitating the generation of wideband responses without demanding extensive spatial requirements [21]. An alternative strategy involves the utilisation of periodically loaded microstrip lines, which incorporate small loading components positioned at uniform intervals along the transmission line. This configuration induces a slow-wave phenomenon, allowing the line to be shortened while achieving equivalent electrical length, thus resulting in marked miniaturisation and an expanded passband [22]. Researchers have expanded their focus beyond traditional rectangular configurations, embracing innovative geometrical forms. Hexagonal resonators are particularly appealing due to their distinctive shape, which facilitates enhanced spatial efficiency and improved frequency response management. Such geometries contribute to achieving compactness while simultaneously enhancing stopband effectiveness [23]. Similarly, structures inspired by fractals utilising recurring patterns at various scales have been utilised to develop filters with adjustable bandwidth and increased frequency attenuation that extends beyond the primary operating range [24].

In [25], a compact UWB filter using a multilayer printed circuit board (MPCB) structure with blind holes and a DGS to improve roll-off rates and in-band return loss. However, the design showed sensitivity to manufacturing tolerances and provided a relatively narrow fractional bandwidth (FBW) of 40.33%. Miniaturized balanced UWB filter on a high-temperature superconducting (HTS) substrate was designed using a composite right-/left-handed (CRLH) transmission line, which achieved an extremely low insertion loss of less than 0.2 dB [26]. A major limitation is the requirement for cryogenic operating temperatures (20 K), and the measured out-of-band rejection was worse than simulated due to fabrication imprecision. A reconfigurable filter is presented in [27] that uses pin diodes to switch between a UWB and a wideband response, achieving a large bandwidth switching range of 6.23 GHz. The drawback was a relatively high insertion loss of up to 1.6 dB and a low roll-off rate in its UWB mode, indicating reduced selectivity. In [28] UWB bandpass filter using a multi-stub-loaded short-circuited ring resonator was designed to generate five resonant modes and achieve a wide FBW of 108.9%. The design's coupling strength was noted to be limited by manufacturing capabilities, which contributed to discrepancies between simulated and measured results. A reconfigurable filter with three switchable quarter-wavelength stubs was designed, enabling five different passbands across four operational states. This versatility came at the cost of inconsistent performance, with some states exhibiting high insertion loss (up to 2.6 dB) and poor return loss [29]. In [30] a hybrid microstrip-to-CPW UWB filter was proposed that uses an MMR in the ground plane to generate multiple transmission zeros for sharp passband roll-offs. While the design achieves good selectivity, its measured insertion loss of up to 1.2 dB is relatively high for a non-reconfigurable filter of this type.

There are many ways to design UWB BPFs, but the existing research still shows some common problems. Many designs face trade-offs such as high insertion loss, low selectivity with slow roll-off, and unstable performance. This creates a clear gap for a UWB filter that can combine high selectivity, low insertion loss, and stable performance while still being simple, low-cost, and easy to manufacture. Using affordable materials like FR4 instead of expensive substrates such as Rogers can make the design much more practical and cost-effective for real-world applications.

In this work, a highly selective UWB BPF has been designed using an interdigital PCML and a honeycomb-shaped resonator. The parallel coupled lines have been modelled using admittance inverter method [31] and honeycomb shaped resonator consist of multiple hexagonal rings and hexagons. Two open stubs are also introduced to increase the selectivity of the filter as well as to increase out-of-band rejection. The filter is simulated and optimized using ANSYS High Frequency Structure Simulator (HFSS) within the frequency range 0.5 GHz to 20 GHz. The filter shows a very good performance in terms of insertion loss, return loss, group delay and out-of-band rejection. The filter has been able to achieve a wide passband from 3.14 GHz to 10.56 GHz along with a fractional bandwidth of 108.32%. Unlike most of the reported filters where expensive low loss substrate materials are used, this work uses high loss and cost-effective substrate material FR4, which can compete with traditional filters by showing high performance with effective and efficient signal transmission.

2 Design Methodology

The honeycomb shaped resonator based UWB BPF is designed in various steps. As the filer is designed using microstrip technology, a suitable substrate material must be selected first. Here, an FR4 substrate with dielectric constant 4.4 and loss tangent 0.02 is chosen due to its versatility, thermal stability and cost effectiveness. The height of the FR4 is taken to be 1.53 mm and a 0.035 mm width copper layer on both sides. A parallel coupled interdigital structure with a central transmission line is designed to achieve a bandpass behaviour using copper on the top layer of FR4 substrate, and the ground layer is filled with copper, as shown in Fig. 1. To excite these parallel coupled lines, 50Ω microstrip transmission line (feed line) is designed on both sides of the structure. The design parameters of this parallel coupled interdigital structure are evaluated using the admittance inverter (J-inverter) method [31, 32]. Then the design is modelled in HFSS software and it is simulated in the frequency range 0.5 GHz to 20 GHz. After optimisation, the dimensional values of width (w) and split gap (s) are found to be $w = 0.2mm$ and $s = 0.2mm$. The transmission (S_{21}) and reflection (S_{11}) characteristics of the filter have been extracted and plotted in Fig. 2. From the plot, it can be observed that the transmission characteristics shows a wide passband of 3 to 10 GHz with -3 dB bandwidth. However, the insertion loss in the passband is too high, and the reflection characteristics achieve a return loss less than 10 dB. Hence, the parallel coupled interdigital structure serves as an initial building block for the UWB BPF, but it needs to be improved in further steps.

Figure 1: interdigital microstrip coupled line structure.

The next step is to use a resonating structure to get a minimum insertion loss in the passband and a sharp transition (higher roll-off) between the passband and stopband. To get the final UWB BPF behaviour, the resonating structure has undergone various changes, shown in Fig. 3 and corresponding transmission and reflection characteristics in Fig. 4 and 5, respectively. A hexagonal ring-shaped structure is embedded in the central transmission line (Fig. 3(a)), resulting in lower insertion loss and higher return loss than the initial interdigital parallel coupled

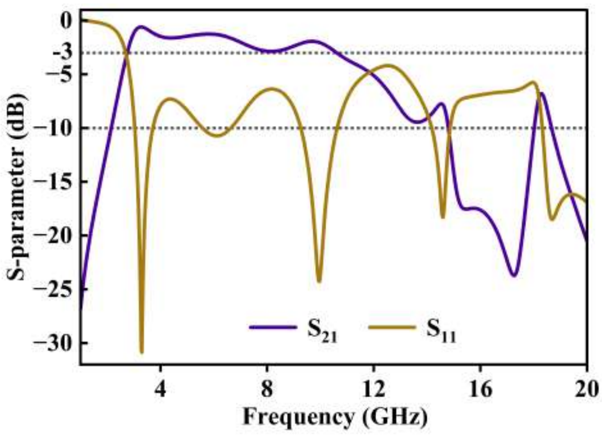

Figure 2: S-parameter response for interdigital coupled line structure.

structure. This structure also shows a lower out-of-band rejection and return loss of 10.37 dB, which needs to be improved in further steps. By using two hexagonal rings instead of a single ring as in Fig. 3(b), wider out-of-band rejection can be achieved, and return loss increases to 12.81 dB. These performances is further improved by adding two inductively coupled hexagonal solid structures in the intermediate space between hexagonal rings without touching the central transmission line, as shown in Fig. 3(c). The return loss found for this structure is 14.94 dB. In the next two steps, the whole structure is covered with hexagonal rings, $i.e.$ first using two more rings as shown in Fig. 3(d) and another four more rings as shown in Fig. 3(e). These neighbouring rings are inductively coupled with each other and the central transmission line. Due to the inclusion of multiple hexagonal rings, the structure looks like a honeycomb structure. This honeycomb structure minimises the insertion loss upto 0.5 dB and maximises the return loss upto 17.1 dB.

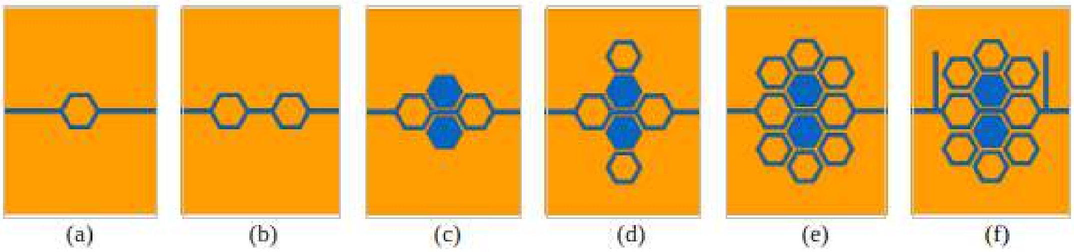

Figure 3: Evolution of the UWB filter.

Finally, at the last stage, two open stubs are placed on both sides of the honeycomb shaped resonator. The inclusion of stubs results in a sharper roll-off in the transition, higher return loss in the passband, and wide out-of-band rejection. These can be clearly observed from Figures 4 and 5. The open stub is optimised for multiple lengths and widths, for which various results are obtained. But the optimum result of s parameter is found at length p = 2.9 mm and width r = 0.2 mm.

The electromagnetic behaviour of the resonator geometry was further analysed using surface current distribution plots for square, circular, and hexagonal configurations, as shown in Fig. 6. It is observed that the hexagonal (honeycomb) resonator exhibits stronger and more uniformly distributed surface current compared to the square and circular structures. The inherent symmetry of the hexagonal structure promotes balanced current flow and stronger confinement of the electric and magnetic fields within the resonator, thereby reducing energy leakage and return loss. In contrast, the square geometry shows current crowding at the corners, resulting in localized field distortion, while the circular geometry exhibits relatively weaker coupling due to limited edge interaction. Consequently, the honeycomb configuration improves field uniformity, suppresses spurious modes, and enhances energy transfer efficiency between the resonator and the feed line, leading to wider bandwidth, lower insertion loss, and improved impedance matching compared to simpler geometries.

After optimising the results for honeycomb shaped resonator, the BPF has been analysed under weak and strong coupling between parallel coupled interdigital lines. This can be done by changing the length a of the

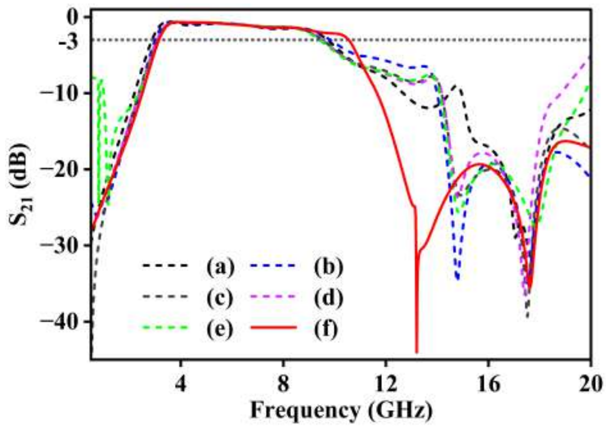

Figure 4: Variation in transmission characteristics.

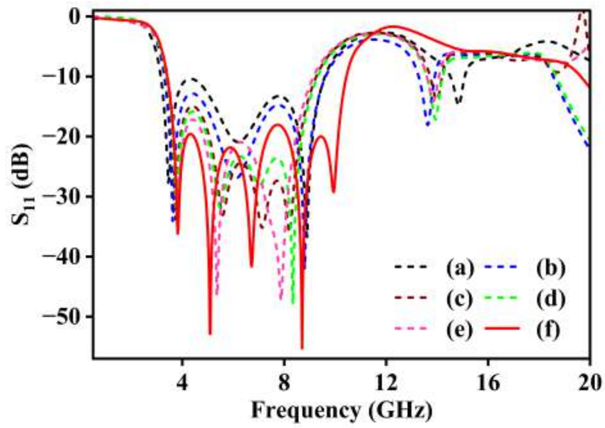

Figure 5: Variation in reflection Characteristics.

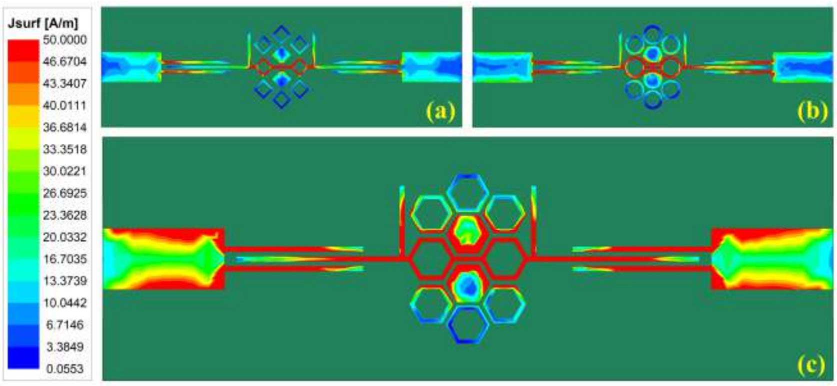

Figure 6: Surface current distribution for (a) Square shaped structure (b) Circular shaped structure (c) Hexagonal shaped structure.

parallel coupled lines. The S_{21} results obtained from this variation with ‘a’ are plotted in Fig. 7. The figure shows that under very weak coupling, the filter shows three resonant modes in 4.64 GHz, 7.10 GHz and 9.56 GHz, respectively. As we increase the coupling by increasing the length a, the insertion loss decreases and a minimum insertion loss of 0.39 dB is obtained for $a = 5.7$ mm. This happens due to the strong coupling between the coupled lines. Also, if we see analytically, a quarter wavelength ($\lambda_g/4$) transmission line gives the best result and strong coupling, where λ_g is the guided wavelength at the centre frequency of the BPF.

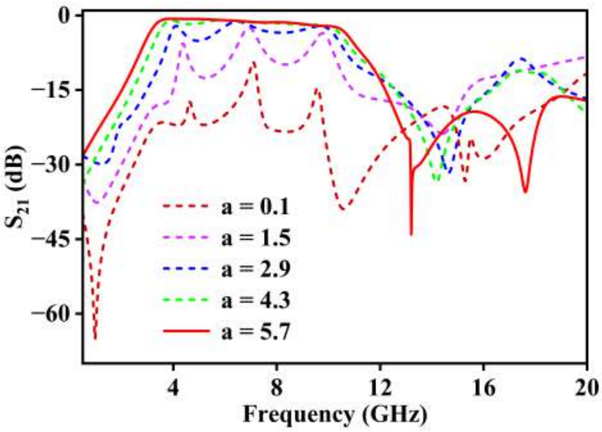

Figure 7: Honeycomb resonator under weak and strong coupling.

3 Results and Discussion

After going through numerous design changes through different steps, the optimised UWB BPF has been demonstrated in Figure 8. In the figure, the filter model is shown with two Sub-miniature version A (SMA) female connectors which will be later used for measurement. The overall dimension of the filter is very small, only $10 \times 30 \times 1.6$ mm^3 or 0.38×1.13 in terms of λ_g. The optimised dimensions of the filter for various parts in the structure are listed in Table 1.

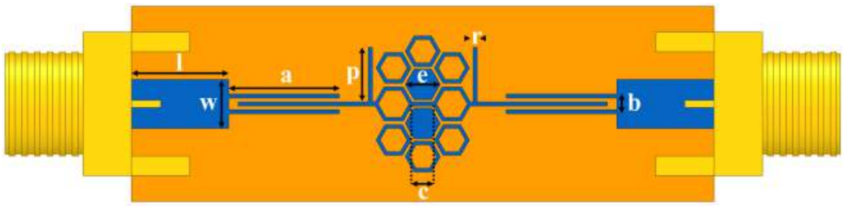

Figure 8: Final design of the UWB filter with ports.

Parameter	Dimension (mm)	Parameter	Dimension (mm)
a	0.2	l	5
b	1.0	p	2.9
c	1.1	r	0.2
e	1.8	w	2.5

Table 1: Optimised dimensions of UWB BPF

In the Fig. 9 the final transmission and reflection characteristics of the UWB filter is plotted within frequency range 0.5 GHz to 20 GHz. From the graph it can be observed that, a wide passband of 3.14 GHz to 10.56 GHz has been achieved by the UWB filter. The insertion loss and return loss in the passband are found to be 0.39 dB and 18.35 dB, respectively which are far better than most of the recently reported works. The bandwidth of the designed filter is 7.42 GHz with fractional bandwidth 108.32% at 6.85 GHz centre frequency. In addition to the wide passband characteristics, the proposed filter exhibits strong out-of-band suppression with steep roll-off at both band edges. Quantitative analysis shows that the stopband rejection levels are approximately -15.02 dB at 12 GHz, -20 dB at 12.86 GHz, -45 dB at 13.2 GHz, -35 dB at 17.5 GHz, and -17.12 dB at 20 GHz. This corresponds to a wide out-of-band rejection bandwidth of about 8 GHz, with minimum attenuation of 15 dB and maximum attenuation of 45 dB. The roll-off rate in the lower transition (1.44 GHz to 3.08 GHz) is 51.49 dB/decade, while in the upper transition (10.62 GHz to 12.86 GHz) it is 204.53 dB/decade. These results confirm the sharp skirt selectivity or sharp roll-off and strong stop band suppression of the proposed filter. To study the time delay between input and output ports, a frequency versus group delay graph is plotted in Fig. 10, where

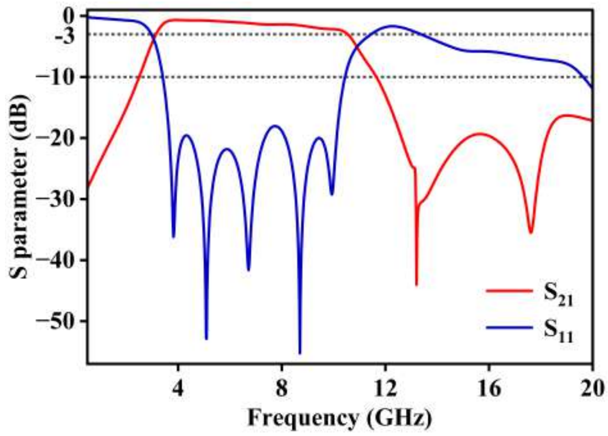

Figure 9: Simulated transmission and reflection Characteristics of UWB filter.

the group delay is taken in the unit nanosecond (ns). The plot shows that the group delay response is almost flat within the passband, around 0.25 ns to 0.3 ns. This shows a smooth and efficient transmission of input signals, maintaining signal integrity.

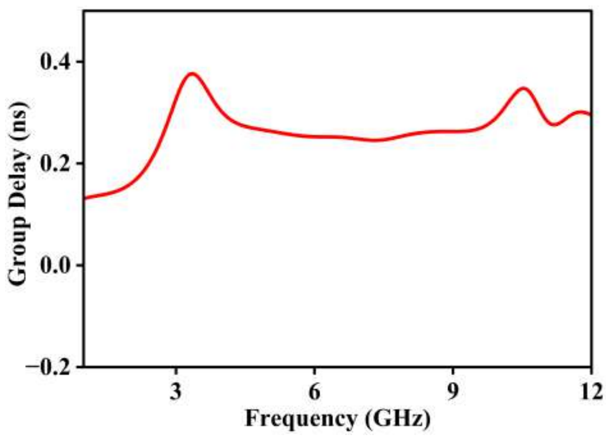

Figure 10: Group Delay of the UWB filter.

The passband and stopband characteristics of the filter can also be verified using surface current density (Jsurf) shown in Fig. 11. The surface current density for the UWB BPF is plotted for two frequencies, one for the centre frequency 6.85 GHz (Fig. 11(a)) and one for a frequency of 13 GHz from the stopband (Fig. 11(a)). From the figure, it can be clearly seen that the current density is uniform throughout the passband throughout the structure. On the other hand, for the stopband the current density vanishes halfway between the structure. From these observations, it can be concluded that the filter works perfectly in the whole frequency range.

To clearly highlight the effectiveness of the proposed honeycomb-shaped UWB filter, a comparative analysis with recently reported works is summarised in Table 2, which presents key parameters such as substrate used, operating passband, centre frequency (Cf), fractional bandwidth (FBW), insertion loss, return loss, group delay, and size of the filter. The table shows that most designs rely on advanced and costly substrates, such as Rogers-made RT/duroid to achieve wide passbands, sharp roll-off, and improved stopband rejection. While these works demonstrate excellent electrical performance, relying on expensive materials often limits their suitability for cost-sensitive applications. On the other hand, the honeycomb-shaped UWB filter presented here is implemented on a low-cost FR4 substrate, which is widely available and practical for mass production. Despite the intrinsic dielectric losses of FR4 at high frequencies, the proposed design successfully achieves a wide operating bandwidth and low insertion loss, comparable to or better than many state-of-the-art UWB BPFs.

As the objective of this work is to establish the design methodology and validate the proposed structure through simulation, all results presented are based on full-wave electromagnetic analysis. The fabrication of the filter and subsequent measurement using a Vector Network Analyzer (VNA) will be carried out in future to experimentally

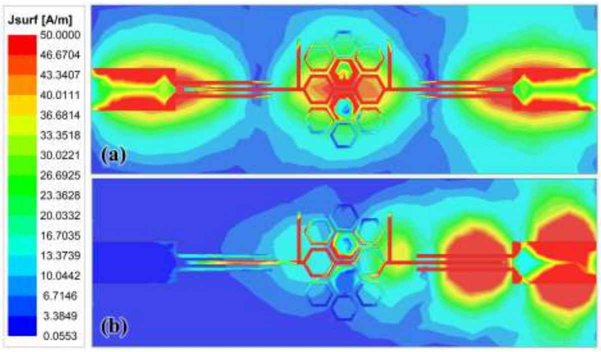

Figure 11: Surface current density at (a) 6.85 GHz and (b) 13 GHz.

confirm the simulated performance. During the practical fabrication of the proposed UWB filter, certain tolerances and material variations may slightly affect the final performance. The dielectric constant of the FR-4 substrate may vary at higher frequencies and the copper cladding thickness may differ due to manufacturing tolerances. Such variations can lead to minor shifts in the passband and small deviations in insertion loss. In addition, parasitic effect due to SMA connector and soldering imperfections may introduce additional losses during measurement. Environmental factors such as temperature and humidity may also cause slight performance fluctuations. These aspects have been considered during the design optimization process, and they will be further examined after prototype fabrication and experimental characterization.

Ref	**Substrate** (ϵ_r)	**Passband (GHz)**	C_f **(GHz)**	**FBW** (%)	**Insertion Loss (dB)**	**Return Loss (dB)**	**Group Delay (ns)**	**Size** ($\lambda_g \times \lambda_g$)
[13]	Rogers RT Duroid 5880 (2.2)	2.30–8.29	5.295	113	0.5	9.7	0.62	–
[19]	FR4 (4.4)	3.11–10.63	6.87	109.4	0.8	–	0.6	0.09×0.43
[25]	Rogers RO4003 (3.55)	3.49–11.04	7.265	103.92	1.95	6	1.73	0.38×1.04
[26]	MRO (9.78)	3.8–8.2	6	72.5	0.2	18.3	–	0.073×0.073
[28]	F4B-2 (3.3)	2.8–9.5	6.15	108.9	0.36	13	0.85	0.41×0.84
[33]	FR4 (4.3)	3–9.5	6.25	104	2	12	0.45	0.43×0.85
[34]	Roger 5880 (2.2)	3.05–10.8	6.925	112	0.5	13	0.8	0.45×0.60
[35]	Rogers RO3003 (3)	3.1–10.7	6.9	110	1.2	10.8	0.4	–
This work	**FR4 (4.4)**	**3.14–10.56**	**6.85**	**108.32**	$>$**0.39**	$>$**18.35**	**0.3**	**0.38×1.13**

Table 2: Comparison of this filter with recently reported works

4 Conclusions

In this work, a compact and highly selective UWB bandpass filter has been successfully designed and demonstrated to overcome common limitations in existing filter designs such as high insertion loss, poor selectivity, and reliance on costly substrates. The proposed filter combines interdigital PCML with a honeycomb-shaped resonator implemented on an economical FR-4 substrate, ensuring both performance and cost-effectiveness. The design achieves a wide operational passband ranging from 3.14 GHz to 10.56 GHz with a fractional bandwidth of 108.32%, while maintaining a minimum insertion loss of 0.39 dB and excellent selectivity characterized by sharp roll-off skirts. Additionally, the filter exhibits a flat group delay response across the passband, which guarantees high signal integrity for broadband applications. Moreover, the unique honeycomb geometry contributes to improved spatial efficiency and compactness. In contrast, other filters frequently employ multilayer configurations, defected ground structures, or fractal shapes to attain similar outcomes. This balance of performance, compactness, and cost-effectiveness establishes the honeycomb resonator filter as a strong alternative to existing solutions for real-world UWB communication systems. This study is presently based on design and full-wave simulation of UWB filter. The fabrication and measurement of the proposed UWB filter will be undertaken in future to experimentally validate its performance. Future research may also explore the integration of tunable notches for interference suppression, particularly for applications in cognitive radio and dynamic spectrum access systems.

Acknowledgements

The authors sincerely acknowledge the DST FIST (level-I) Project No (SR/FST/PSI-217/2016) and the DST PURSE Project No (SR/PURSE/2022/143) and funding by the Department of Science & Technology, Govt. of India to the Department of Physics, Dibrugarh University, Assam, India for financial assistance.

References

[1] J. Hong and M. J. Lancaster, *Microstrip Filters for RF/Microwave Applications*, 1st ed. (John Wiley & Sons Ltd, 2001).

[2] D. M. Pozar, *Microwave Engineering*, 4th ed. (Wiley, 2011).

[3] A. I. Zverev, *Handbook of Filter Synthesis* (Wiley-Interscience, 2005).

[4] X. Gao and L. Huai, Int. J. Ultra Wideband Commun. Syst. **4**, 57 (2020).

[5] P. P. Kalita *et al.*, *Advances in Microwave Engineering: From Novel Materials to Novel Microwave Applications*, edited by A. Bhattacharya *et al.* (CRC Press, Boca Raton, 2023), pp. 297–315.

[6] M. NoroozOliaei, in *Wideband Wave-Propagating Components for Wireless RF Communications*, edited by M. Alibakhshikenari (IntechOpen, 2025).

[7] H. Nikookar and R. Prasad, *Introduction to Ultra Wideband for Wireless Communications* (Springer Netherlands, Dordrecht, 2009), pp. 1–10.

[8] S. Yan, P. J. Soh, and G. A. E. Vandenbosch, IEEE Access **6**, 42177 (2018).

[9] F. Che *et al.*, Sensors **23**, 5710 (2023).

[10] P. P. Kalita *et al.*, in *2024 15th International Conference on Computing Communication and Networking Technologies (ICCCNT)* (IEEE, Kamand, India, 2024), pp. 1–6.

[11] A. Basit, A. Daraz, and G. Zhang, Micromachines **14**, 1986 (2023).

[12] F. M. Alnahwi *et al.*, Electronics **10**, 450 (2021).

[13] X.-F. Li and J.-K. Xiao, AEU - International Journal of Electronics and Communications **175**, 155100 (2024).

[14] Q. Li and T. Yang, IEEE Trans. Microwave Theory Tech. **69**, 65 (2021).

[15] S. Udhayanan and K. Shambavi, Prog. Electromagn. Res. Lett. **117**, 41 (2024).

[16] G. Saxena, P. Jain, and Y. K. Awasthi, Int. J. Microw. Wireless Technol. **13**, 999 (2021).

[17] M.-H. Weng *et al.*, Electronics **9**, 209 (2020).

[18] P. Chakraborty *et al.*, Prog. Electromagn. Res. M **108**, 89 (2022).

[19] P. P. Shome and T. Khan, Microsyst. Technol. **26**, 2295 (2020).

[20] B. Sahu, in *2020 6th International Conference on Signal Processing and Communication (ICSC)* (IEEE, Noida, India, 2020), pp. 71–73.

[21] S. M. A. Motakabber and M. N. Haidari, Int. J. Electr. Comput. Eng. **8**, 1654 (2018).

[22] C. Yang *et al.*, J. Phys.: Conf. Ser. **2480**, 012005 (2023).

[23] M. Popov *et al.*, Sci. Rep. **13**, 1179 (2023).

[24] N. Radhi and M. Fadhil, Int. J. Wirel. Mob. Networks **15**, 09 (2023).

[25] C. Li *et al.*, Electronics **12**, 1728 (2023).

[26] H. Tian, H. Liu, and Z. Song, IEEE Microw. Wirel. Technol. Lett. **33**, 1607 (2023).

[27] A. Bandyopadhyay, P. Sarkar, and R. Ghatak, IEEE Trans. Circuits Syst. II **69**, 2747 (2022).

[28] G. Wei, Y. Wang, J. Liu, and H. Li, ACES Journal, **38**, 496 (2023).

[29] S. Ramkumar and R. Boopathi Rani, AEU-Int. J. Electron. Commun. **151**, 154219 (2022).

[30] A. N. Ghazali, M. Sazid, and B. Virdee, Microw. Opt. Technol. Lett. **60**, 1925 (2018).

[31] P. P. Kalita *et al.*, AEU - Int. J. Electron. Commun. **191**, 155682 (2025).

[32] G. L. Matthaei, L. Young, and E. M. T. Jones, *Microwave Filters, Impedance-Matching Networks, and Coupling Structures* (Artech House, 1980).

[33] H. Louazene, M. Challal, and M. Boulakroune, Prog. Electromagn. Res. Lett. **109**, 75 (2023).

[34] M. Bod and S. M. Hashemi, IETE J. Res. **70**, 4415 (2023).

[35] K. Aliqab, Sci. Rep. **14**, 15669 (2024).